JOURNAL OF OPTOELECTRONİCS AND ADVANCED MATERİALS Vol. 8, No. 5, October 2006, p. 1867 - 1873

Influence of the indium incorporation on the structural and electrical properties of zinc oxide films

YASEMIN CAGLAR*, MUHSIN ZOR, MUJDAT CAGLAR, SALIHA ILICAN
Deparment of Physics, Faculty of Science, Anadolu University, Eskisehir, 26470, Turkey

Undoped and indium-doped ZnO films have been deposited onto glass substrates by the spray pyrolysis method. The effect of indium incorporation on structural and electrical properties of ZnO films has been investigated. Zinc acetate dihydrate, indium chloride were used as a starting material and a dopant source, respectively. X-ray diffraction pattern of the films showed hexagonal wurtzite type polycrystalline structure. The results show that indium incorporation leads to substantial changes in the structural characteristics of ZnO films. The grain size was found to be in the range 15-50 nm, depending on indium content. In addition, the surface morphology features of the films, as a function of the indium content, are shown. For all the films, a linear dependence typical of ohmic behavior was observed. The electrical conductivity of ZnO films was improved by indium incorporation. The most important changes were observed for 1 at.% In-doped ZnO film which exhibit a resistivity of 3.2×10^{-1} Ωcm. At certain constant voltage, from Arrhenius plots of In-doped ZnO films, activation energy values have been calculated from 17 meV to 89 meV.

(Received August 8, 2006; accepted September 13, 2006)

Keywords: Zinc oxide, Indium incorporation, X-Ray diffraction, Electrical properties

1. Introduction

Due to their significant properties, which are electro-optical properties, high electro-chemical stability, a large band gap, abundance in nature and absence of toxicity, zinc oxide (ZnO) semiconductor films have been extensively investigated and have received considerable attention in recent years. ZnO is suitable for use in devices such as gas sensors, heat mirrors, transparent electrodes, solar cells and piezoelectric devices [1-5].

The electrical properties of ZnO films can be controlled by incorporation it with appropriate impurities, usually the Group-III elements, which are indium, aluminum and gallium [6-8]. The choice of the type of impurity has to take into account, among other conditions, the size of the ionic radius of the impurity that has to be similar to the ion that it substitutes in order to avoid lattice distortions. The addition of impurities to ZnO is improved by replacing Zn^{2+} atoms with the atoms of elements of higher valency. The efficiency of the dopant element related to its electronegativity and the ionic radius.

Numerous In-doped ZnO films preparation methods have been attempted: pulsed magnetron sputtering, electrodeposition process, sol–gel method, electrostatic spray deposition and spray pyrolysis [3, 6, 13, 14]. Among these methods, the spray pyrolysis method has several advantages over the others such as simplicity, safety and the low cost of the apparatus and the raw materials. This method is based on the preparation of solutions of some salt of the material whose films is to be prepared. The films obtained by this method are suitable for many scientific studies and technological applications. We deposited II-VI compounds [15, 16] by spray pyrolysis method.

Electrical properties of ZnO films have been widely investigated. However, very little is known about activation energy studies of In-doped ZnO films. In this paper, in order to improve the film properties, we present the effect of indium incorporation on the structural and electrical properties of ZnO films deposited by the spray pyrolysis method.

2. Experimental

The undoped and In-doped ZnO films were deposited onto glass substrates, chemically cleaned, using the spray pyrolysis method at 350 ^{o}C substrate temperature. 0.1 M solution of zinc acetate dihydrate ($Zn(CH_3COO)_2.2H_2O$) diluted in methanol and deionized water (3:1) was used for all the films, and indium chloride ($InCl_3$) was added to starting solution for indium doping. The In/Zn ratio was 0 at.%, 1 at.%, 3 at.%, and 5 at.%. A few drops of acetic acid were added to improve the clarity of solution. The schematic diagram of the spray pyrolysis apparatus used in this work is shown in Fig. 1. Nitrogen was used as the carrier gas, pressure at 0.2 bar. The ultrasonic nozzle to substrate distance was 28 cm and during deposition, solution flow rate was held constant at 4 $mlmin^{-1}$.

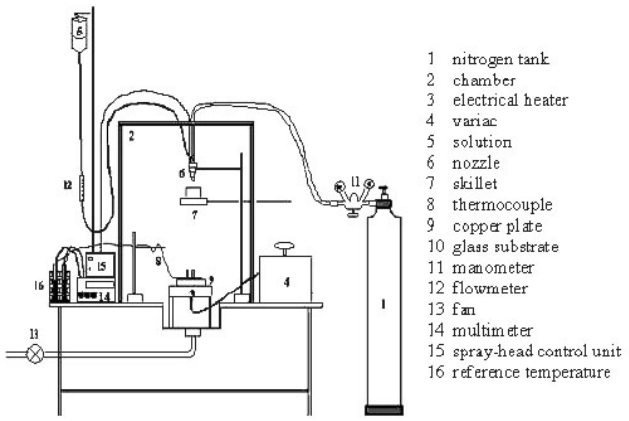

Fig. 1. Schematic of the spray pyrolysis system used for the films.

Surface morphology was studied using ZEISS SUPRA 50VP model scanning electron microscope (SEM). The structural analysis of all the films was performed with RIGAKU RINT 2200 Series X-Ray Automatic Diffractometer with CuK_α (λ=1.5405 Å) radiation. Electrical contacts were made by gold electrodes on the surfaces of the films using vacuum evaporation method (Leybold Heraus 300 Univex system). Electrical measurements have been carried out in dark, in vacuum of 3×10^{-3} mbar and at temperatures in the range between 188-300 K using Oxford Instruments 43305 Cryostat and Hewlett Packard 4140B pA meter/dc Voltage Source. The films were found to be n-type as determined from hot probe method.

3. Results and discussion

3.1. Structural and morphological properties

The crystal structure and orientation of the undoped and In-doped ZnO films were investigated by X-ray diffraction (XRD) patterns. Fig. 2 shows the diffraction patterns of all the films. As seen in Fig. 2, the films are polycrystalline with hexagonal wurtzite type structure. The crystallinity of ZnO films decreases when the indium doping concentration increases.

As shown in Fig. 2.a, undoped film has (002) as the preferred orientation. Another major orientation present is (101), while other orientations like (100), (102) and (110), are also seen with comparatively lower intensities.

From X-ray diffraction spectra of In-doped ZnO films (Fig. 2.b-d) it is clear that all the doped films have (101) as the preferred orientation. The other peaks present are (002), (100), (102) and (110). Indium incorporation in to the compounds caused reorientation which exhibited itself as (101) preferred orientation, whereas (002) peak intensities observed to be decreased.

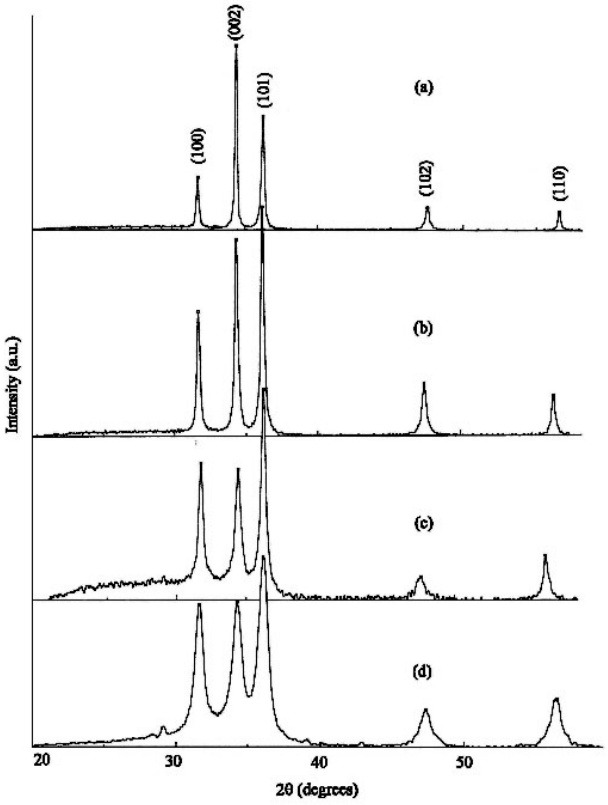

Fig. 2. X-ray diffraction spectra of (a) undoped, (b) 1 at.% In-doped, (c) 3 at.% In-doped, and (d) 5 at.% In-doped ZnO films.

The relative percentage error for the observed and JPCDS standard *d-values* for all the films are calculated using the formula [17]

$$Relative\ percentage\ error = \frac{|Z_H - Z|}{Z} x100 \qquad (1)$$

where Z_H represents the actual obtained *d-value* and Z is the standard *d-value* in JCPDS card file. For all the films *2θ, d-values*, and *d% error* data calculated by using eq. (1) are given in Table 1. The average relative percentage error is found to be 0.25%, 0.23%, 0.06%, and 0.44% for the undoped, and 1 at.%, 3 at.%, and 5 at.% In-doped ZnO films respectively. The experimental *d-values* and JCPDS *d-values* are in relatively good agreement and show hexagonal structure [18].

The lattice constants for hexagonal ZnO film are reported in JCPDS standart data a=3.24982 Å and c=5.20661 Å [18]. The analytical method [19] for calculating lattice constants is used to calculate a and c for all the films (Table 2). These calculated values are aggrement with JCPDS data.

Table 1. 2θ, d-values and calculated d% error for the films.

	Undoped ZnO			1 at.% In-Doped ZnO			3 at.% In-Doped ZnO			5 at.% In-Doped ZnO		
(hkl)	2θ	d(Å)	d% error	2θ	d(Å)	d% error	2θ	d(Å)	d% error	2θ	d(Å)	d% error
(100)	31.767	2.8145	0.72	31.680	2.8220	0.27	31.780	2.8134	0.03	31.620	2.8273	0.46
(002)	34.379	2.6064	0.12	34.340	2.6093	0.23	34.440	2.6019	0.05	34.260	2.6152	0.46
(101)	36.221	2.4780	0.25	36.160	2.4820	0.25	36.260	2.4754	0.02	36.040	2.4900	0.57
(102)	47.500	1.9126	0.08	47.440	1.9148	0.19	47.560	1.9103	0.04	47.340	1.9187	0.40
(110)	56.541	1.6264	0.10	56.480	1.6279	0.20	56.520	1.6269	0.14	56.420	1.6295	0.30

Table 2. Lattice constant values of the films.

	Undoped ZnO	1 at.% In-Doped ZnO	3 at.% In-Doped ZnO	5 at.% In-Doped ZnO
a (Å)	3.24990	3.25856	3.24863	3.26468
c (Å)	5.21280	5.21860	5.20380	5.23040

The grain size of crystallites was calculated using a well-known Scherrer's formula [19]:

$$D = \frac{0.9\lambda}{\beta \cos\theta} \tag{2}$$

where D is the grain size of crystallite, λ (=1.5405 Å) the wavelength of x-rays used, β the broadening of diffraction line measured at half its maximum intensity in radians and θ the angle of diffraction. The values found for the grain size are in the range 15-50 nm which agrees with the values reported in the literature [3, 20].

The grain size values of all the films are shown in Table 3. It can be seen that as long as the indium content increases the grain size of the films decreases. This behavior of the grain size increasing the doping level is in agreement with those reported for ZnO thin films prepared by the same process [21, 22]. This effect can be explained if it is considered that (i) indium atoms do not substitute zinc ions, instead they occupy interstitial sites resulting in a large number of dislocations and (ii) probable formation of compound which is growing along with ZnO:In.

Table 3. Preferentially oriented planes and grain size variations of ZnO films with indium content.

Sample Name	Plane	Grain size (nm)
Undoped ZnO	(002)	49.20
1 at.% In-Doped ZnO	(101)	37.16
3 at.% In-Doped ZnO	(101)	30.96
5 at.% In-Doped ZnO	(101)	15.44

The texture coefficient (*TC*) represents the texture of the particular plane, deviation of which from unity implies the preferred growth. The different texture coefficient TC(hkl) have been calculated from the x-ray data using the well-known formula [23]

$$TC(hkl) = \frac{I(hkl)/I_o(hkl)}{N^{-1}\sum_n I(hkl)/I_o(hkl)} \tag{3}$$

where *I(hkl)* is the measured relative intensity of a plane *(hkl)*, $I_o(hkl)$ is the standard intensity of the plane *(hkl)* taken from the JCPDS data, *N* is the reflection number and *n* is the number of diffraction peaks. *TC(hkl)* values of all the films are presented in Table 4.

Table 4. Relative intensity of the peaks (I/I_o) and TC(hkl) values of the films.

	Undoped ZnO		1 at.% In-Doped ZnO		3 at.% In-Doped ZnO		5 at.% In-Doped ZnO	
(hkl)	I/Io	TC(hkl)	I/Io	TC(hkl)	I/Io	TC(hkl)	I/Io	TC(hkl)
(100)	28	0.6667	54	0.9640	65	1.2548	75	1.2668
(002)	100	2.3810	86	1.5357	62	1.1969	76	1.2837
(101)	61	1.4524	100	1.7857	100	1.9305	100	1.6892
(102)	12	0.2857	23	0.4107	11	0.2123	20	0.3378
(110)	9	0.2143	17	0.3035	21	0.4054	25	0.4222

The variation of texture coefficient for (002) and (101) planes with the indium content is shown in Fig. 3. It can be seen that the highest *TC* values have been obtained for (002) peak of undoped ZnO film and for (101) plane of

all the doped films. It is interesting to note that *TC*(002) decreases continuously with increasing indium content, while *TC*(101) shows increase with indium content.

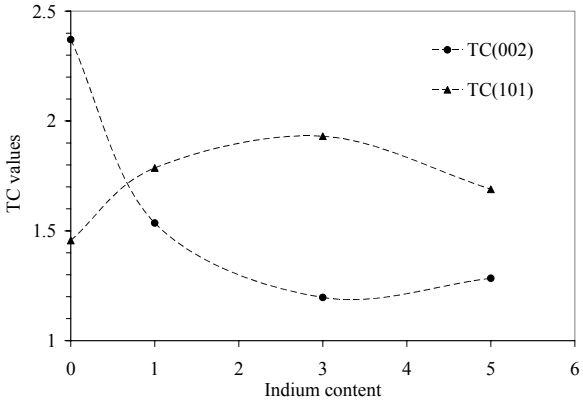

Fig. 3. Variation of TC (002) and TC (101) with indium content in ZnO films.

Fig. 4a-d show scanning electron micrographs of the undoped and In-doped ZnO film at 40000 magnifications. It was seen that the surface morphologies of ZnO films were almost homogeneous. It shows continuous coverage of the substrate with microcrystals. Here also, it can be noticed that the microstructure of the films is influenced by the introduction of indium atoms as dopant. Generally, the films surface morphology show a porous structure consisting of grains separated by empty spaces. For undoped film, the film is composed of regular grains with approximately 200 nm average diameter. Depending on the increasing indium concentration, the surface morphologies of the films were deteriorated. This result supports the XRD observations and shows the transition of the material from crystalline to amorphous structure. These SEM micrographs show different morphologies of the surface grains, which depend on indium concentration. The c-axis orientated structure of the films chances to normal random orientation structure, due to the grain agglomeration, as seen in the SEM micrographs.

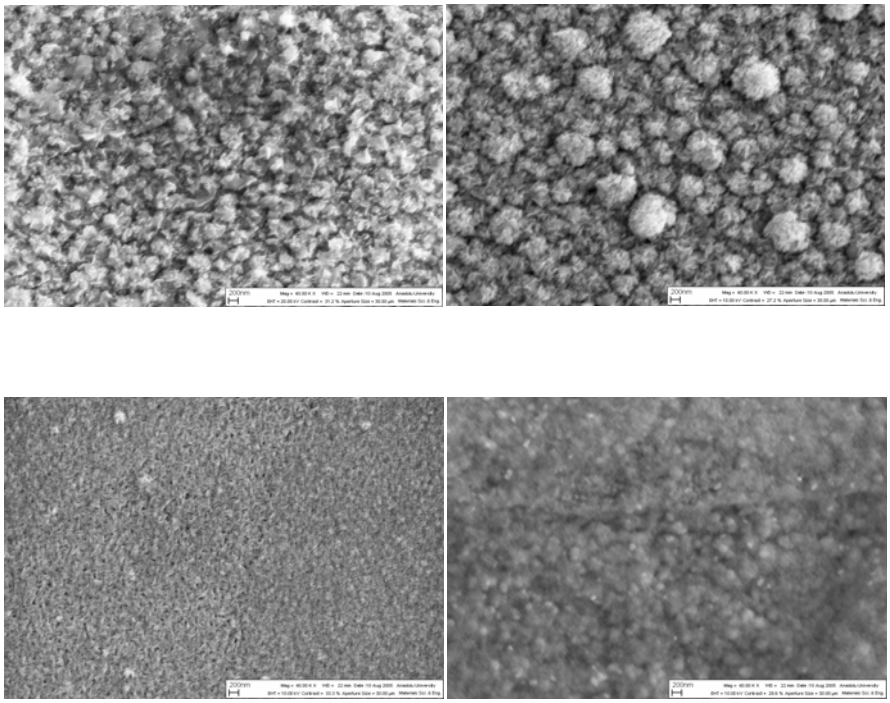

Fig. 4. Scanning electron micrographs (SEM) of (a) undoped, (b) 1 at.% In-doped, (c) 3 at.% In-doped, and (d) 5 at.% In-doped ZnO films.

The optical absorption spectra of undoped and In-doped ZnO films at room temperature were recorded on a SHIMADZU UV-2101 PC UV-VIS Spectrophotometer in the wavelength range 200-900 nm, but not presented here. The direct band gaps of undoped, and 1 at.%, 3 at.%, and 5 at.% In-doped ZnO films were calculated as 3.15, 3.18, 3.17 and 3.10 eV, respectively. An initial increase in the optical band gap (E_g) values could be attributed to the indium atoms incorporated into the ZnO lattice. ZnO is naturally n-type material and the Fermi level will be inside of the conduction band, when it is doped with indium, that is, the lowest states of the conduction band will be partially filled, due to the increase of carrier concentration in the ZnO film. The partial filling of the conduction band leads to a blocking of the lowest states and hence a widening to the optically observed band gap. The widening of the E_g is generally attributed to the Burstein-Moss shift. The effect is observed for at. %In ≤1. On the other hand, it was seen that the higher indium content caused to decrease in the E_g values. The trend of decreasing on the E_g for %In>1 could be attributed to the poor crystallinity of the prepared films or to the formation

of the new compound based on In and Zn. More details about optical properties of undoped and In-doped ZnO films are given elsewhere [24].

3.3. Electrical properties

Important characterizations include electrical conductivity and the interface behavior of the semiconductor with various metals for photovoltaic application.

Electrical properties of undoped and In-doped ZnO films including the electrical resistivity, conduction mechanism and activation energy were carried out. Hot probe method was used in order to determine conductivity type. It was seen that all the films exhibit n-type conductivity. It is well known that n-type conductivity in undoped ZnO is due to the oxygen vacancy and interstitial zinc atom, which act as donors [25].

A logarithmic plot of the current (I) as a function of the applied voltage (V) is shown in Fig. 5 for undoped and In-doped ZnO films at room temperature. The curves have a slope of approximately unity at 1volt, implying that the conduction is ohmic in this voltage.

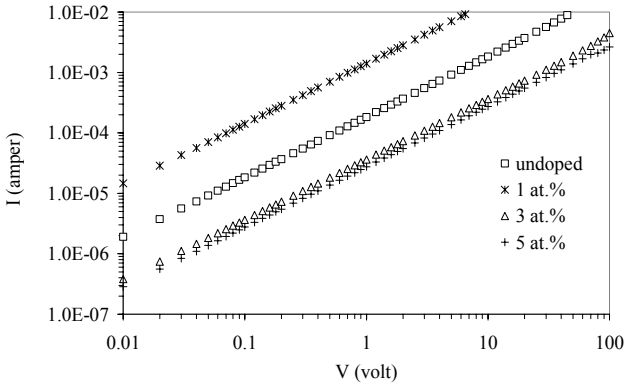

Fig. 5. The I-V characteristics of the films at room temperature.

Electrical resistivity measurements have been carried out using the two-probe method. The electrical resistivity of ZnO films as a function of indium content are plotted in Fig. 6. The calculated resistivity values are in good agreement with the literature data [17, 26]. It is shown that indium content is a parameter affects the electrical properties of these films. It is seen that as indium is added to the starting solution, the electrical resistivity first decreases and then increases. A lower resistivity value was obtained at 1 at.% In-doped ZnO film. An initial decrease in the resistivity is due to an increase in the free-electron concentration with indium incorporation in the ZnO film. In the other words, it can be attributed to the optimal incorporation of indium atoms into the lattice, increasing the donor concentration and contributing to a decrease of the resistivity. Afterwards, the increase observed in the electrical resistivity with the subsequent addition of indium to the starting solution could be also attributed to the reduction in the grain size which reduces the majority carrier mobility because of increasing the scattering process. The adding more indium in the starting solution will increase the indium concentration in the film, then the high indium concentration will also increase the scattering process and therefore the majority carrier mobility is decreased.

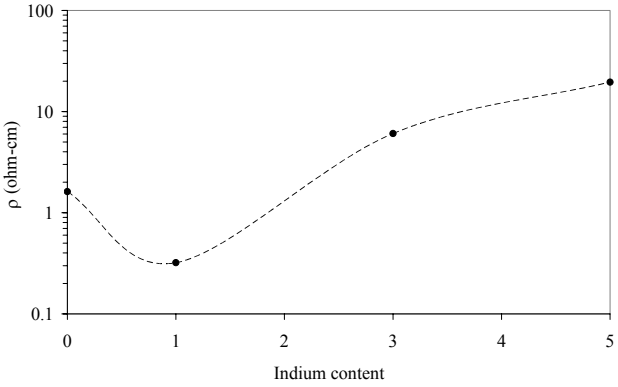

Fig. 6. The electrical resistivity of ZnO films as a function of indium content.

The linear relationship between the logarithm of conductivity and inverse of temperature with a negative slope indicates that the following well-known Arrhenius law is satisfied

$$\sigma = \sigma_0 \, exp(-\Delta E/kT) \tag{4}$$

where σ_0 is is a constant for a given material, ΔE is activation energy, T is absolute temperature and k is Boltzmann constant. We may write

$$ln\,\sigma = ln\,\sigma_0 + (-\Delta E / kT) \tag{5}$$

or

$$ln\sigma = -(\Delta E/1000k)(1000/T) + ln\,\sigma_0 \tag{6}$$

When we plot a graph between $ln\sigma$ and $1000/T$, a straight line is obtained having slope $(\Delta E=1000k)$ and intercept $ln\sigma_0$. Thus, the activation energy can be calculated by using the slope of the straight line.

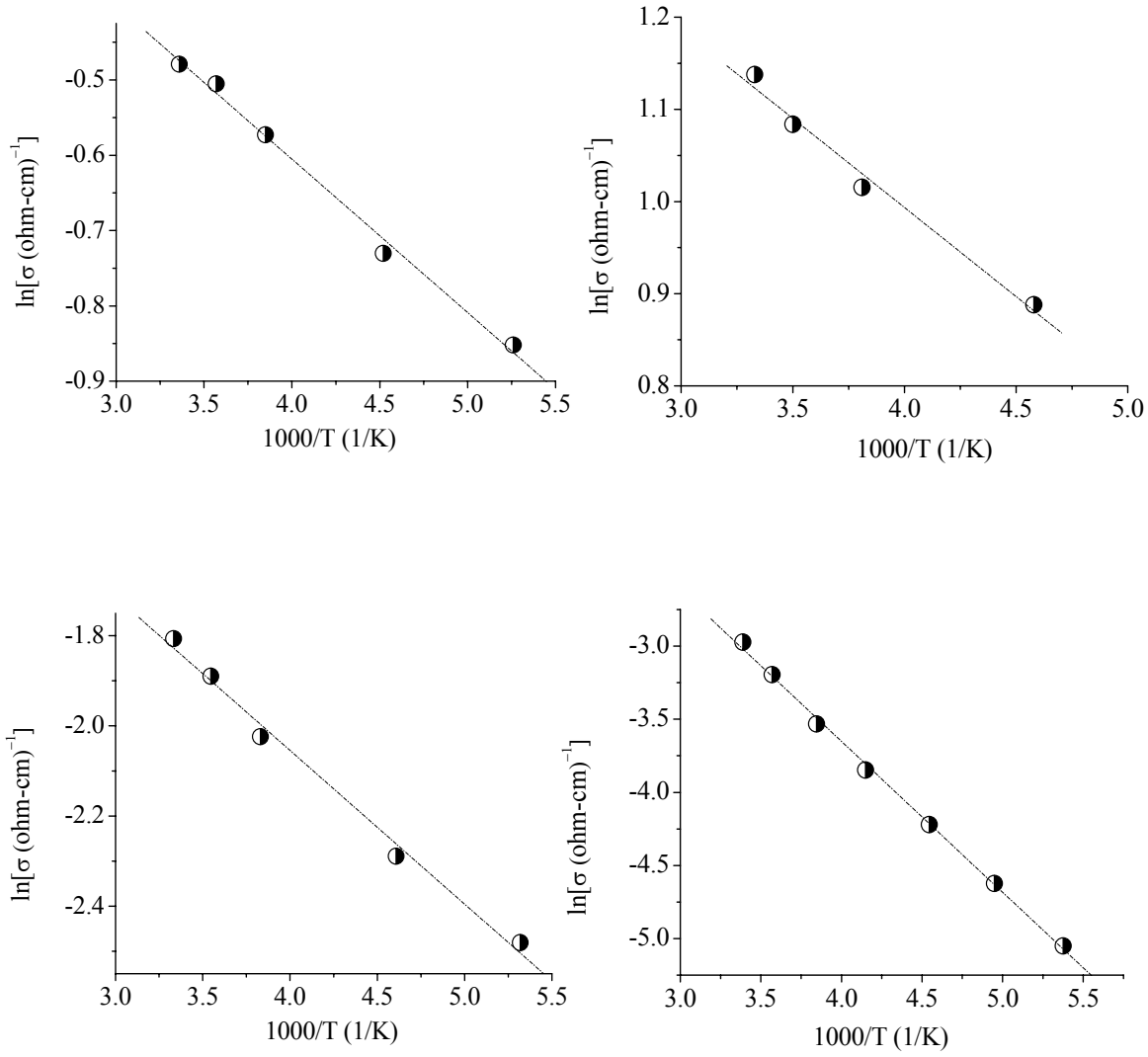

Fig. 7. The ln (σ [Ωcm]$^{-1}$) ~ 1000/T (1/K) characteristics of (a) undoped, (b) 1 at.% In-doped, (c) 3 at.% In-doped, and (d) 5 at.% In-doped ZnO films.

The electrical conductivity of the deposed films was measured in dark, in the range of temperature from 188 to 300 K were measured. The temperature dependence of the conductivity is shown in Fig. 7a-d. The conductivity of all these films increases with increase in temperature. The plots of $ln\sigma$ against $1000/T$ are straight lines for all the films indicating that conduction in these films is through thermally activated process. The activation energy values is estimated to be 18 meV, 17 meV, 29 meV, and 89 meV for the undoped, and 1 at.%, 3 at.%, and 5 at.% In-doped ZnO films respectively. These values could be attributed to the donor levels formed by interstitial zinc atoms and ionization energies of oxygen vacancies stated in literature [27]. Furthermore, the activation energies increasing by indium incorporation have been considered to be closely related to the impurity band may be likely formed. It is interesting to note that, the increasing on the ΔE and the decreasing on the E_g by indium incorporation are the same.

4. Conclusions

From this work, the following conclusions may be drawn:

(i) Undoped and In-doped ZnO films were deposited by the spray pyrolysis method at 350 ^{o}C substrate temperature. The effects of indium incorporation on structural and electrical properties of ZnO films was investigated.

(ii) All the deposited films are polycrystalline in nature. No phases corresponding to indium oxide or to other indium compounds were detected. The crystalline nature of the films was deteriorated with indium incorporation. Furthermore the preferential orientation of ZnO films also changed from (002) to (101), grain sizes decreased depending on the indium incorporation. It was found that a decrease in grain size with incorporation of indium.

(iii) The scanning electron micrographs showed that the surface morphology is affected by the indium content. Depending on the increasing indium concentration, the surface morphologies of the films were deteriorated.

(iv) The *I-V* curves show that all the films exhibit ohmic conduction mechanism.

(v) The indium incorporation affects the resistivity of ZnO films. The 1 at.% In-doped film had a lower resistivity than other films and its value was $3.2x10^{-1}\Omega cm$.

(vi) The activation energy increases with the increase of indium content percentage in ZnO film. The activation energy values are 17-89 meV in the temperature range of 188-300 K and at 1 V.

Consequently, it was seen that indium incorporation makes a significant change on the structural and electrical properties.

Acknowledgement

The financial support of T.R. Prime Ministry State Planning Organisation is gratefully acknowledged (project no. 97K120390). The authors are grateful to Anadolu University Department of Materials Science and Engineering for the XRD and SEM measurements.

References

[1] P. Mitra, A.P. Chatterjee, H.S. Maiti, Mater. Lett. **35**, 33 (1998).

[2] K. L. Chopra, S. Major, D. K. Pandya, Thin Solid Films **102**, 1 (1983).

[3] S. Major, A. Banerjee, K. L. Chopra, Thin Solid Films **143**, 19 (1986).

[4] J. B. Yoo, A. L. Fahrenbruch, R. H. Bube, J. Appl. Phys. **68**, 4694 (1990).

[5] J. G. E. Gardeniers, Z. M. Rittersma, G. J. Burger, J. Appl. Phys. **83**, 7844 (1998).

[6] H. Gomez, A. Maldonado, R. Asomozo, E. P. Zironi, J. Canetes-Ortega, J. Palacios-Gomez, Thin Solid Films **293**, 117 (1997).

[7] S. Ghosh, A. Sarkar, S. Chaudhuri, A. K. Pal, Thin Solid Films **205**, 64 (1991).

[8] X. Yu, J. Ma, F. Ji, Y. Wang, C. Cheng, H. Ma, Applied Surface Science **245**, 310 (2005).

[9] Y. Zhou, P. J. Kelly, A. Postill, O. Abu-Zeid, A. A. Alnajjar, Thin Solid Films **447–448**, 33 (2004).

[10] G. Machado, D. N. Guerra, D. Leinen, J. R. Ramos-Barrado, R. E. Marotti, E. A. Dalchiele, Thin Solid Films **490**, 124 (2005).

[11] E. J. Luna-Arredondo, A. Maldonado, R. Asomoza, D. R. Acosta, M. A. Melendez-Lira, M. de la L. Olvera, Thin Solid Films **490**, 132 (2005).

[12] B. G. Choi, I. H. Kim, D. H Kim, K. S. Lee, T. S. Lee, B. Cheong, Y.-J. Baik, W. M. Kim, Journal of the European Ceramic Society **25**, 2161 (2005).

[13] M. S. Tokumoto, A. Smith, C. V. Santilli, S. H. Pulcinelli, A. F. Craievich, E. Elkaim, A. Traverse, V. Briois, Thin Solid Films **416**, 284 (2002).

[18] M. Krunks, E. Mellikov, Thin Solid Films **270**, 33 (1995).

[14] P. Nunes, E. Fortunato, R. Martins, Thin Solid Films **383**, 277 (2001).

[15] M. Caglar, M. Zor, S. Ilican, Y. Caglar, Czech, J. Phys. **56**, 277 (2006).

[16] S. Ilican, M. Zor, Y. Caglar, M. Caglar, Optica Applicata **36**, 1 (2006).

[17] D. P. Padiyan**,** A. Marikani, Cryst. Res. Technol. **37**, 1241 (2002).

[18] Joint Committee on Powder Diffraction Standards, Powder Diffraction File, card no: 36-1451.

[19] B. D. Cullity, S. R. Stock, Elements of X-Ray Diffraction, Prentice Hall, 2001, 3nd ed.

[20] Y. Ohya, H. Saiki, Y. Takahashi, Journal of Materials Science **29**, 4099 (1994).

[21] A. Sanchez-Juarez, A. Tiburcio-Silver, A. Ortiz, E. P. Zironi, J. Rickards; Thin Solid Films **333**, 196 (1998).

[22] A. Sanchez-Juarez, A. Tiburcio-Silver, A. Ortiz, Solar Energy Materials and Solar Cells **52**, 301 (1998).

[23] C. S. Barret, T.B. Massalski, Structure of Metals, Pergamon Press, Oxford,1980.

[24] M. Caglar, Ph.D. Thesis, Anadolu University, Turkey, 2002, p. 56.

[25] M. G. Ambia, M. N. Islam, M. Obaidulhakim, Journal of Materials Science **29**, 6575 (1994).

[26] K. Haga, P. S. Wijesena, H. Watanabe, Applied Surface Science **169-170**, 504 (2001).

[27] L. Koudelka, J. Horak, P. Jariabka, Journal of Materials Science **29**, 1497 (1994).

*Corresponding author: yasemincaglar@anadolu.edu.tr